Numerical Simulation of the Lateral Frequency Response of a Thin Cantilever Beam-Like Structure by Using the Finite Element Model

Dojoong Kim[1] and Tae-Gun Jeong[2,*]

[1] Department of Mechanical and Automotive Engineering, University of Ulsan, San-29, Mugeo-dong, Nam-gu, Ulsan, 680-749, Korea
djkim@ulsan.ac.kr
[2] School of Mechanical Engineering, Konkuk University, 1 Hwayang-dong, Gwangjin-gu, Seoul 143-701, Korea
tgjeong@konkuk.ac.kr

Abstract. One of the main obstacles of high track density is the confined servo bandwidth due to the low resonant frequencies of the mechanical components. We study the dynamic characteristics of the actuator system with a thin cantilever beam-like structure by using the finite element analysis. We develop the finite element models of each components of the actuator system and analyze the dynamics of the overall actuator system. The frequency response analysis shows that the modes regarding to the pivot bearing dominate in the lateral response. The lateral and vertical responses at the dimple point are compared with those for the suspension model to study the dynamic characteristics of a coupled structure.

Keywords: Finite Element Method, Frequency Response, Coupled Structure, Thin Cantilever Beam.

1 Introduction

The capacity and performance of HDDs (hard disk drives) have been increased significantly since the introduction of the IBM RAMAC 350, the first random access device, at 1957 [1], [2]. Recording density as an important capacity index depends directly on the linear and track densities. Recent products have recording density of 1.5 Gb/in^2 with track density of 15k tpi (tracks per inch) and linear density of 100k bpi (bits per inch). There are many technical problems to improve the track density [3]. Among others, the bandwidth of a tracking servo system has to be increased without losing the stability of the slider air bearing. Early products employed the linear type actuator that drove the actuator longitudinally to position the head on the disk. Although this kind of system drives the actuator along the linear guide with minimal friction, the driving mechanism is too complicated and too heavy to decrease the seek time sufficiently. The rotary type actuator was introduced to reduce the physical size of the disk drive and the inertia of the actuator [4].

* Corresponding author.

O. Gervasi and M. Gavrilova (Eds.): ICCSA 2007, LNCS 4706, Part II, pp. 895–906, 2007.

The rotary type actuator positions the head in radial direction by rotating it about the pivot by the torque supplied at the VCM (voice coil motor). In actual system, one or two suspensions are attached to each arm. Driving current at the VCM surrounded by permanent magnets generates the magnetic field proportional to the strength of the current and the number of winding of the coil. This magnetic field determines the direction of the force that drives the actuator system. The rotary type actuator with a VCM usually leads to the smaller size HDD with simpler structure and larger driving force.

Comparing to the linear actuator, the rotary type actuator has small inertia in the driving direction due to the concentrated mass around the pivot. The structure needs short bearing operation distance resulting in the extended bearing life. However, driving in radial direction excites the actuator system in lateral direction resulting in a large off-track error. The rotary type actuator has low stiffness in operating direction while the linear actuator has high stiffness [4]. The rotary type actuator employs truss structure and laterally wide design in order to increase the lateral stiffness and to reduce the rotational inertia [5]. The rotary type actuator with in-line suspension where the air bearing pad is parallel to the suspension, is structurally weak to the lateral excitation, for example, the lateral bending and sway modes [6]. The sway mode affects the track error most significantly. The natural frequency of the sway mode decreases as the bending angle and bending ratio increase [7].

The suspension dynamics has been studied for the fixed base plate, which ignores the effects of the VCM and actuator arm. We develop the finite element model for the actuator system and perform the modal analysis to compare the results with those considering the suspension only and to investigate the effects of each part on the suspension dynamics. The analysis is done for the free and loaded suspensions. E-block is considered for the fixed and pivot bearing cases. We do the modal analysis of the whole actuator system by assembling each part for the pivot bearing case. The frequency response analysis by using the finite element model of the actuator system is necessary to understand the dynamics in detail. We calculate the lateral displacement for the lateral excitation to study the dynamic characteristics of the actuator system. To know the dynamic characteristics of the pivot bearing, the VCM, and the arm, we compare the frequency response function of the whole actuator system with that of the suspension or E-block model.

2 Modal Analysis of Coupled Structure System

2.1 HGA

Structure. An HGA (head-gimbal assembly) is composed of the suspension (load beam), flexure (gimbal), and slider (Figure 1). The dynamic characteristics of the HGA are very important to improve the track density because the HGA is the most flexible structure that supports the read/write head. In this study, we employ the type 850 LSF (laterally stiff flexure) suspension by Hutchinson and the NPAB (negative

pressure air bearing) slider by Seagate. The length of the suspension is 18 mm, the thickness 0.076 mm, and ribs are attached at both sides to increase the bending stiffness. The compliance becomes worse while the natural frequency of the bending mode becomes higher due to the rib. The suspension is attached to the base plate by the seven points of spot welding. The base plate is to connect the suspension to the actuator arm. The flexure of 0.0305 mm thickness is attached to the end of the suspension by the two points of spot welding. It connects the suspension and the slider and makes the motion of the slider compliant to that of the disk.

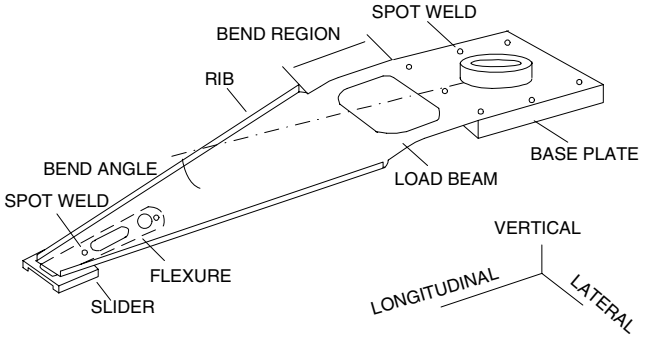

Fig. 1. Structural Components of an Head-Gimbal Assembly

Finite Element Model. The natural frequency of the deflection mode of the slider made of ceramic is much higher than that of the HGA structure. We model the slider with the simple rectangular element since its deflection has little effect on the suspension dynamics that is lower than 20 kHz. We used 792 elements with 1050 nodes to model the HGA. The points of spot welding are represented by node-sharing to prevent the relative motion. The multi-point constraints are employed to supplement the lack of the constraint force because the actual welding point has finite size. Table 1 shows the material properties used in the finite element analysis.

Table 1. Material properties of the HGA

	Material	Young's modulus (GPa)	Density (kg/m^3)	Poisson's ratio	Thickness (mm)
Base plate	Stainless steel	193	8020	0.32	
Load beam	Stainless steel	193	7890	0.32	0.078
Bend region	Stainless steel	193	7890	0.32	0.04
Flexure	Stainless steel	193	7890	0.32	0.0305
Slider	Al_2O_3-TiC	393	4220	0.23	

Modal Analysis Results. At the free case, the slider and the suspension are not subject to the air bearing. We model the free case by clamping only the base plate. Table 2 shows the modal and experimental analysis results for the free case.

Table 2. Modal analysis results for the free case (FEM and experiment)

Description	FEM (Hz)	Experiment (Hz)	Difference (%)
1st Bending	171.6	179.6	-4.45
Slider Pitch	1160.9		
Slider Roll	1218.1	1356.6	-10.21
2nd Bending	2309.7	2419.1	-4.52
1st Torsion	2465.5	2609.6	-5.52
3rd Bending	6918.8	6591.9	4.96
Sway	7098.9	7124.4	-0.36
2nd Torsion	7743.2	7629.0	1.50

The differences are less than 5% except the slider modes. The sway mode shows less than 1% difference. The first three modes are the compliance modes that help slider follow the disk surface. The modes after the second bending are the tracking stiffness modes related to the tracking error. A suspension should be designed to have low natural frequencies of compliance modes for the stable air bearing and to have higher frequencies of tracking stiffness modes for the wide bandwidth of the tracking servo system. These two conflicting design requirements are difficult to satisfy.

Table 3. Modal analysis results for the loaded and free cases (FEM)

Description	Loaded (Hz)	Free (Hz)	Difference (%)
2nd Bending	2053.0	2309.7	-11.11
1st Torsion	2296.7	2465.5	-6.85
3rd Bending	6205.0	6918.8	-10.32
Sway	6844.7	7098.9	-3.58
2nd Torsion	7380.6	7743.2	-4.68

At the loaded case, the slider flies on the disk maintaining the constant gap (less than 50 nm) sustained by the load transferred from the suspension and the air bearing pressure. The loaded case is modeled by the displacement boundary condition at the corners of the slider. Table 3 shows the finite element analysis results for the free and loaded cases. The natural frequencies for the bending modes decrease more than 10% at the loaded case.

2.2 E-Block

Modal Testing. E-block transfers the driving force proportional to the current supplied to the VCM and determines the accurate position of the suspension. High-stiffness material minimizes the amplitude of vibration. Uniform distribution of the rotational inertia about the pivot axis minimizes the unbalance. Low-density material minimizes the rotational inertia leading to less power consumption and faster access.

Measured open-loop transfer function for a usual HDD shows the lowest resonant frequency around 3.5 kHz. We can predict that the mode corresponding to this frequency causes the tracking error. But there has been no accurate analysis on this fact. At least, however, we can say that it has nothing to do with the suspension. Here we measure the dynamics of the E-block to investigate the governing mode.

The E-block considered here is composed of four arms (aluminum) and the VCM support (VECTRA) that has very low mass density. The VCM coil and the support are integrated by the injection molding of VECTRA differently from the conventional E-block in which the VCM coil is attached to the support by adhesive bond.

Experimental method is similar to the modal testing for the free case of the suspension. E-block is secured to the shaker by the tapped end of a jig shaft. We measure the excitation input to the system by the accelerometer attached at the jig and measure the output response by the LDV. Tight connection between the shaker and the E-block reduces the external disturbance to the system giving the more accurate results. For the LDV, we have to use retro-reflective tape to get the good signal. We attach the tape at 76 points. We choose the random input of small magnitude for the E-block not to rotate by the excitation force. The excitation signal should have sufficient power to excite the high frequency modes without the rotation of the bearing by shock. Vertical excitation gives a good cross-spectrum in the vertical direction. However, the lateral response is too weak to obtain satisfactory response at all frequency bands. The VCM part of the E-block considered in this study is thinner than the conventional type and has two holes around the center to decrease the total mass and the rotational inertia. There appear many combined modes of the arms and the VCM after the E-block bending mode (1.82 kHz). The twisting, bending and the membrane modes of the VCM appear at 5.04, 5.13, and 6.91 kHz, respectively.

Finite Element Analysis. Each arm has thin truss structure for high lateral stiffness and low rotational inertia. The VCM support has the same thickness as the coil and laterally wide shape for high lateral stiffness. We develop the finite element model of the E-block with 2122 elements and 3818 nodes. The model ignores wire and its support, bearing, small manufacturing holes, and the step of the arm and the VCM support. The connection between the arm and the VCM support is modeled by sharing the degree of freedom of the contact surfaces. The material properties used at the finite element modeling are shown at Table 4. The pivot bearing has radial stiffness of 12.8 MN/m and axial stiffness of 45.6 MN/m. It is modeled by solid elements and the one-dimensional spring elements. We use eight spring elements in radial direction and four in axial direction.

Table 4. Material properties of the E-block

Material	Young's modulus (GPa)	Density (kg/m^3)	Poisson's ratio
Aluminum alloy	75	2755	0.33
VECTRA	10	1470	0.33
Copper	80	8490	0.33

The fixed case is analyzed to compare with the experimental results to verify the finite element model of the E-block. The boundary conditions for the fixed case are to constrain the degree of freedom at the jig contact area. Table 5 shows the comparison results.

Table 5. Experimental and FEM analysis results for the fixed case

Description	FEM (Hz)	Experiment (Hz)	Difference (%)
1^{st} Bending (VCM)	741	717	3.35
1^{st} Bending (Arm 1,4 in-phase)	1293	1270	1.81
1^{st} Bending (Arm 1,4 out-of-phase)	1313	1300	1.00
1^{st} Torsion (VCM)	1616		
1^{st} Bending (Arm 2,3 in-phase)	1893	1820	4.05
1^{st} Bending (Arm 2,3 out-of-phase)	1961		
1^{st} Bending (E-block)	3776	3210	17.63
2^{nd} Bending (E-block)	3785	3820	-0.92
3^{rd} Bending (E-block)	5659	5130	10.31
1^{st} Torsion (E-block)	5890	5450	8.07
2^{nd} Torsion (E-block)	6543	6410	2.08
Torsion (Arm 1,4 out-of-phase)	6664		
Torsion (Arm 1,4 in-phase)	6794		
Membrane (VCM)	7433	6910	7.55
Lateral bending (Arm out-of-phase)	8136		

Compared to the VCM modes, arm modes show little difference between the experiment and analysis. It is due to the inaccurate material properties of the VECTRA and insufficient representation of the shrinkage connection between the VCM support and the arm area. Arms of same thickness show in-phase and out-of-phase modes. The in-phase mode of the inner arms affects the other part of the system while the motion of the outer arms is independent. Even the simple bending mode has twisting effect at the shorter side and the twisting mode has the lateral bending effect because of the unsymmetrical shape of the arm. We also analyze the pivot bearing condition to study the actuator dynamics at the operating condition. The rigid body mode at the axial direction appears due to the pivot bearing modeling. The results for the pivot bearing case will be described at the whole actuator system analysis.

2.3 Actuator System

Finite Element Model. We develop the finite element model of the actuator system after assembling the suspension and the E-block. Modal analysis is done for the free and loaded condition for the pivot bearing case. Since the relatively large suspension displacement makes the mode shapes of the E-block less identifiable at the overall model, we identify the mode shape of the suspension and E-block separately by animation.

Modal Analysis Results. The modes of slider pitch, slider roll, and the first suspension bending show the in-phase and out-of-phase modes for the arms of the same thickness. The flexure modes appear from 8 kHz to 10 kHz. Table 6 shows that the natural frequency of the first bending mode decreases by about 4% due to the effect of the arm. The modes of slider pitch and roll do not change significantly because they do not depend on the boundary condition of the suspension. The tracking modes like the sway and the second twisting show large change due to the assembly. At the E-block part, the twisting mode and the lateral bending mode appear around 7 kHz where the sway mode appears for the analysis of the suspension only. These modes are coupled together by the assembly resulting in low natural frequency of the sway mode. The modes for the suspension attached to the thinner arm come earlier than for the other arms. The sway and third bending modes show relatively large discrepancy after assembly, which is due to the structural coupling between the suspension and E-block.

Table 6. FEM analysis results of an actuator system for the free case (suspension part)

Description	Actuator system model (Hz)	Suspension model (Hz)	Difference (%)
1st Bending	165~167	172	-4.1
Slider Pitch	1147~1178	1158	-1.0
Slider Roll	1209~1212	1215	-0.5
1st Torsion	2115~2134	2310	-8.4
2nd Bending	2359~2527	2465	-4.3
Sway	4873~5885	7096	-31.3
3rd Bending	6172~6875	6917	-10.8
2nd Torsion	7239~7474	7732	-6.4

Table 7 shows the results for the E-block part. Arm modes show the reduced natural frequencies. The rigid body modes at the low frequency show little difference. The lateral modes of arms show the natural frequencies decreased by 10-17% revealing that the lateral stiffness becomes weaker due to the assembly. In this case, the first bending modes (in-phase and out-of-phase) show large discrepancy after assembly. E-block part is very susceptible to bending mode coupling.

Table 7. FEM analysis results of an actuator system for the free case (E-block part)

Description	Actuator system (Hz)	E-block (Hz)	Difference (%)
Rocking	729	731	-0.3
1st Bending (Arm 1,4 in-phase)	889	1285	-30.8
1st Bending (Arm 1,4 out-of-phase)	905	1313	-31.1
Torsion (VCM)	1603	1602	0
Bending (E-block)	3671	3693	-0.6
Bending (E-block)	5360	5615	-4.5
Torsion (Arm 1,4 out-of-phase)	6172	7714	-20.0
Torsion (Arm 1,4 in-phase)	6358	7387	-14.0
Lateral bending (Arm)	7009	8440	-17.0
Lateral bending (Arm)	7044	8463	-16.8
Lateral bending (Arm)	8577	8547	0.4
Torsion (Arm 2,3 in-phase)	9553		
Torsion (Arm 2,3 out-of-phase)	9973	9453	5.5

3 Frequency Response Analysis

The frequency response analysis by using the finite element model is to identify the modes that contribute to the track error. The FRFs (frequency response functions) for the suspension and E-block are calculated and compared with those for the actuator system. The analysis for suspension is done by a lateral excitation with all degrees of freedom for the base plate fixed. We use a force equivalent to the VCM torque to calculate the responses of the E-block and actuator system.

3.1 Suspension

Boundary Conditions. We calculate the lateral and vertical responses of the slider and suspension for the lateral excitation at the base plate which is fixed. Figure 2 represents the boundary conditions. The responses are calculated at the six points including the dimple point. We exclude the coupled motion by obtaining the responses along the longitudinal center line of the suspension.

Frequency Response Analysis. Figure 3(a) shows the lateral FRFs for the free and loaded cases. The natural frequencies of the sway and the second twisting modes are lower at the loaded case. The magnitude of the twisting mode is larger at the free case while that of the sway mode is larger at the loaded case. Figure 3(b) shows the vertical FRFs at the dimple point. There occur big differences both at the resonant frequencies and magnitude. The first bending mode disappears for the loaded condition. The magnitude of the second bending mode is larger both for the free and loaded cases. Magnitude gain in average decreases more than 70 dB at the loaded case.

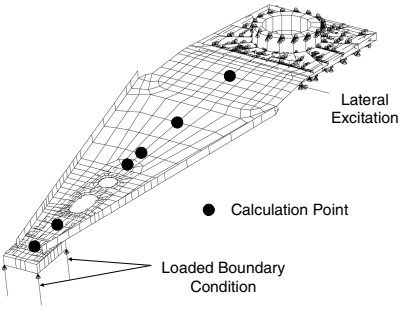

Fig. 2. Boundary Conditions for the Lateral Frequency Response Analysis

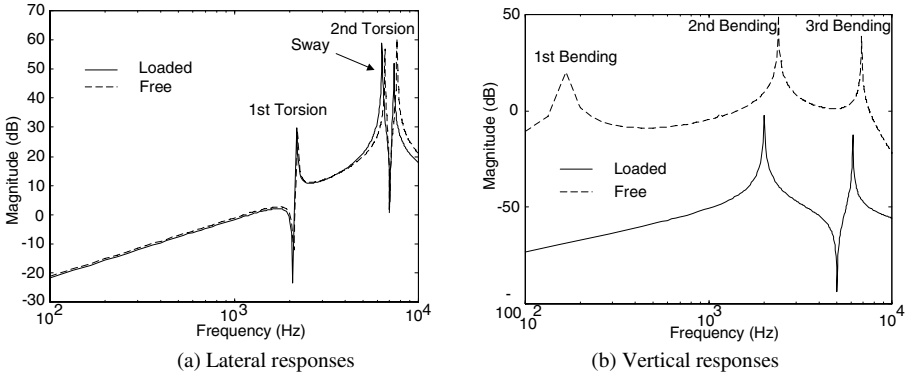

(a) Lateral responses (b) Vertical responses

Fig. 3. FRFs of the Suspension for the Free and Loaded Cases

3.2 E-Block

Boundary Conditions. Figure 4 represents the VCM excitation as an equivalent force tilted by 5° to model the input force considering the shape of the VCM. We calculate the lateral and vertical displacement responses at the six points of the arm, the pivot bearing, and the VCM with respect to the lateral excitation.

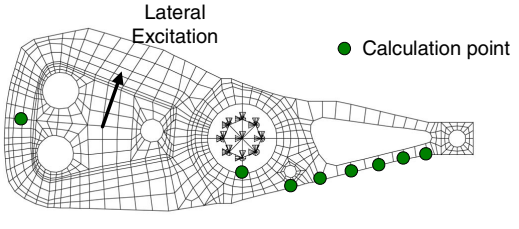

Fig. 4. Finite element model for the FRF analysis of an E-block

Frequency Response Analysis. We represent the lateral and vertical responses at the tip of the arm along with those at the VCM as in Figure 5 in order to compare the frequency responses at each parts of the E-block. The tip of the arm and the VCM show similar response at low frequency range. The stiffness of the pivot bearing causes the lateral bending mode of the E-block, which is the first mode that limits the bandwidth of the tracking servo. Each part shows different characteristics for the vertical responses. The VCM and the arm show large response at the rocking mode and the first bending mode, respectively. The maximum vertical response appears at the frequency where the effect of the pivot bearing is the greatest.

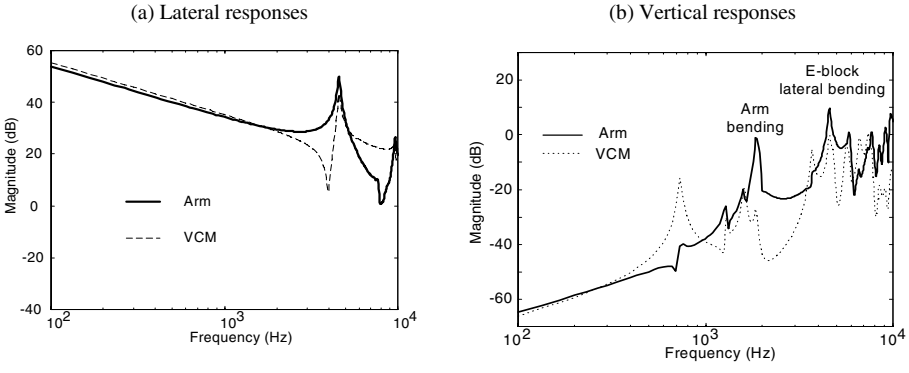

Fig. 5. FRFs of the E-block

Actuator System. We calculate the responses for the lateral excitation for the loaded and free cases when the suspension is assembled with the arm. The points of calculation are the same as the case of suspension and E-block. The excitation force and the calculation range are also the same as the previous cases. In order to investigate the characteristics of the arm with the suspension, we compare the analysis results of the E-block only and the actuator system for the free case. Figure 6(a) is the frequency response function at the tip of the arm. The lateral bending modes of the arm appear at 4.5 and 8.8 kHz for the E-block only and 4 and 5.2 kHz for the actuator system. For the sway and second twisting modes, the natural frequencies decrease by 10 and 70%, respectively, while the gain increases more than 80 dB in both cases. Increased mass and length due to the attachment of the suspension cause the reduction of the lateral stiffness. We observe the effect of the pivot bearing at the actuator system too. However, there appears the mode due to the suspension in addition to the mode due to the pivot bearing.

We compare the analysis with the experimental results for the identical condition at Figure 6(b). In the experiment, the VCM excites the actuator system laterally and the LDV measures the velocity of the slider to obtain the FRF. We observe a significant effect of the pivot bearing in both results. We cannot find the first twisting mode of the suspension in the experimental results. For sway mode, both the natural frequency

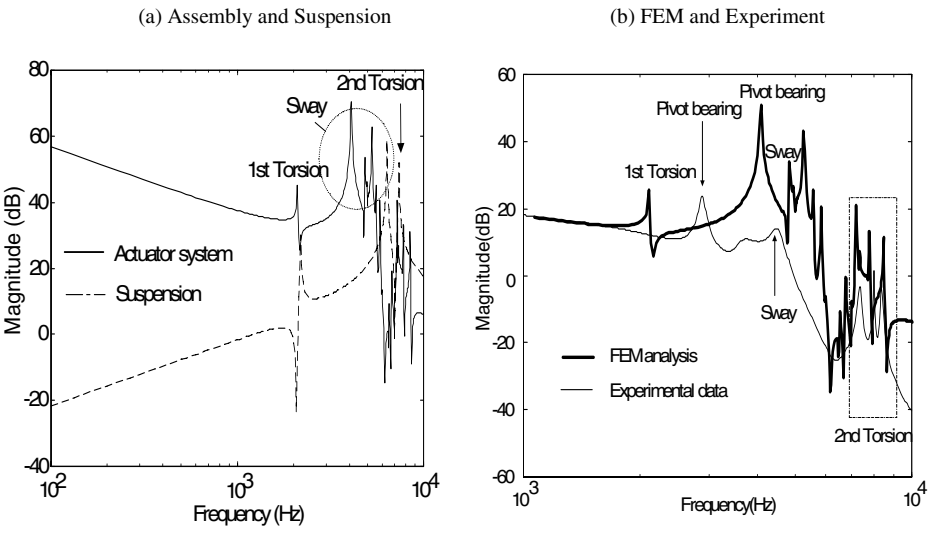

Fig. 6. Comparison of the lateral FRFs

and gain change a lot because of the effect of the pivot bearing. Both results agree well except for the pivot bearing and sway modes.

4 Summary

We analyze the dynamics of the HDD actuator system including the suspension by FEM modal and frequency response analyses.

Modal analysis of the E-block gives the rotational and translational rigid body modes due to the pivot bearing. The natural frequency of sway mode decreases by 30% as the lateral bending and suspension sway modes occur together. Natural frequencies after assembling are lower in general. Same modes appear repetitively in adjacent frequency range due to the duplicate shape of the arm and suspension.

Frequency response analysis of the suspension shows little difference between the sway and second twisting modes in lateral responses while those for the vertical responses show big difference. The lateral response for the E-block shows that the rigid body mode due to the pivot bearing is important. The pivot bearing mode shows the largest gain also for the vertical response.

Frequency response analysis of the actuator system shows that the difference between the sway and second twisting modes becomes large due to the pivot bearing. From the experimental and FEM analysis results, we find that the pivot bearing is the most important element to determine the bandwidth of the tracking servo system.

Acknowledgments. This paper was supported by Konkuk University in 2006.

References

1. Noyes, T., Dickinson, W.E.: The Random-Access Memory Accounting Machine, II. The Magnetic-Disk, Random-Access Memory. IBM Journal of Research and Development 1, 72–75 (1957)
2. Grochowski, E., Hoyt, R.F.: Future Trends in Hard Disk Drives. IEEE Transactions on Magnetics 32, 1850–1854 (1996)
3. Oswald, R.K.: Design of a Disk File Head-Positioning Servo. IBM Journal of Research and Development 18, 506–512 (1974)
4. Heath, J.G.: Design of a Swing Arm Actuator for a Disk File. IBM Journal of Research and Development 20, 389–397 (1976)
5. Winfrey, R.C., Riggle, C.M., Bernett, F., Read, J., Svendsen, P.: Design of a High Performance Rotary Positioner for a Magnetic Disk Memory. IEEE Transactions on Magnetics MAG-17(4), 1392–1395 (1981)
6. Henze, D., Karam, R., Jeans, A.: Effects of Constrained-Layer Damping on the Dynamics of a Type 4 In-line Head Suspension. IEEE Transactions on Magnetics 26(5), 2439–2441 (1990)
7. Jeans, A.H.: Analysis of the Dynamics of a Type 4 Suspension. ASME Journal of Vibration and Acoustics 114, 74–78 (1992)